

KA-TP-02-96  
February 1996

# Loop Induced Higgs Boson Pair Production at $e^+e^-$ Colliders.

A. DJOUADI\*, V. DRIESEN AND C. JÜNGER

Institut für Theoretische Physik, Universität Karlsruhe,  
D-76128 Karlsruhe, FR Germany.

## Abstract

We analyse the loop induced production of Higgs boson pairs at future high-energy  $e^+e^-$  colliders, both in the Standard Model and in its minimal supersymmetric extension. The cross sections for Standard Model Higgs pair production through  $W/Z$  boson loops,  $e^+e^- \rightarrow H^0H^0$ , are rather small but the process could be visible for high enough luminosities, especially if longitudinal polarization is made available. In the Minimal Supersymmetric Standard Model, the corresponding processes of CP-even or CP-odd Higgs boson pair production,  $e^+e^- \rightarrow hh, HH, Hh$  and  $e^+e^- \rightarrow AA$  have smaller cross sections, in general. The additional contributions from chargino/neutralino and slepton loops are at the level of a few percent in most of the supersymmetric parameter space.

---

\*Supported by Deutsche Forschungsgemeinschaft DFG (Bonn).

## 1. Introduction

The search for scalar Higgs particles and the exploration of the electroweak gauge symmetry breaking sector will be one of the main goals of future high-energy colliders. While Higgs particles will probably be first produced at the Large Hadron Collider LHC, the clean environment of high-energy  $e^+e^-$  linear colliders would be required for a detailed investigation and for the high-precision measurement of the fundamental properties of the Higgs particles [1], a crucial requirement to establish the Higgs mechanism as the basic mechanism to generate the masses of the known particles. To this end, a precise calculation of the branching ratios of all important decay channels as well as the cross sections of the production mechanisms, is mandatory [1, 2].

The main production mechanisms of the Standard Model (SM) Higgs particle  $H^0$  at high-energy  $e^+e^-$  colliders [2], are the bremsstrahlung process [3],  $e^+e^- \rightarrow H^0Z$ , and the vector boson fusion mechanisms [4],  $e^+e^- \rightarrow W^*W^*/Z^*Z^* \rightarrow H^0\nu\bar{\nu}/H^0e^+e^-$ . Besides providing the experimental signals for the Higgs particles, these processes would also allow to measure the Higgs couplings to gauge bosons, and to test that they are indeed proportional to the  $W/Z$  masses, a fundamental prediction of the Higgs mechanism. Some of the couplings of Higgs particles can also be measured by considering the decay branching ratios [5] or higher-order production processes. For instance, the Higgs boson self-coupling can be accessible in the pair production processes  $e^+e^- \rightarrow H^0H^0Z$  and/or  $W^*W^*/Z^*Z^* \rightarrow H^0H^0$  [6], while the Yukawa coupling of light Higgs bosons to top quarks can be directly measured in the process  $e^+e^- \rightarrow t\bar{t}H^0$  [7].

Higher order processes might also be useful to discriminate between the Higgs sector of the Standard Model from the usually more complicated scalar sectors of its possible extensions. Among these extensions, supersymmetric theories and in particular the Minimal Supersymmetric Standard Model (MSSM) are the most natural, theoretically. In the MSSM, the Higgs sector is enlarged to contain two scalar doublet fields leading to a spectrum of five Higgs particles: two neutral CP-even ( $h$  and  $H$ ), a CP-odd ( $A$ ) and two charged ( $H^\pm$ ) Higgs bosons [1]. In the decoupling regime [8], where the  $A, H$  and  $H^\pm$  bosons are very heavy, the lightest Higgs boson  $h$  has exactly the same properties as the SM Higgs boson, except that its mass is restricted to be smaller than  $M_h \lesssim 140$  GeV.

If the genuine supersymmetric particles were too heavy to be kinematically accessible in collider experiments, the only way to distinguish between the SM and the lightest MSSM Higgs boson in this limit, is to search for loop induced contributions of the supersymmetric particles, which could give rise to sizeable deviations from the predictions of the SM. Well known examples of this loop induced processes are the  $\gamma\gamma$  widths of the Higgs particles [which can be measured in the decay  $H \rightarrow \gamma\gamma$  at hadron colliders, and more precisely at high-energy  $e^+e^-$  colliders in the direct production of Higgs particles via laser-photon fusion,  $\gamma\gamma \rightarrow \text{Higgs}$ ] or the process  $e^+e^- \rightarrow Z+\text{Higgs}$  which in the MSSM receive extra contributions from supersymmetric gaugino and sfermion loops [9, 10, 11].

Another type of such discriminating processes is the pair production of Higgs bosons which will be analyzed in this paper. In the Standard Model, where it has been first

discussed in Ref.[12], the process

$$e^+e^- \rightarrow H^0H^0 \quad (1)$$

is mediated only by  $W$  and  $Z$  boson loops, Fig.1a, while in the Minimal Supersymmetric extension, additional contributions to the corresponding process

$$e^+e^- \rightarrow hh \quad (2)$$

will originate from chargino, neutralino, selectron and sneutrino loops, as well as loops built up by the associated  $A$  and  $H^\pm$  bosons; Fig.1b. At high center-of-mass energies,  $\sqrt{s} \gtrsim 1$  TeV, the cross sections of the processes are rather small, being of the order of a fraction of a femtobarn. However, with the large luminosities expected at these colliders,  $\int \mathcal{L} \gtrsim 100 \text{ fb}^{-1}$ , and with the availability of longitudinal polarization of the electron and positron beams which could increase the cross sections by a factor of four, a few hundred events might eventually be collected in the course of a few years, allowing for the experimental study of this final state<sup>1</sup>.

The supersymmetric contributions to the process  $e^+e^- \rightarrow hh$  in the MSSM turn out to be rather small compared to the dominant  $W/Z$  [and  $A/H^\pm$ ] contributions. Except in some regions of the SUSY parameter space where they can reach the level of  $\sim 15\%$ , they are typically of the order of a few percent, rendering the distinction between the SM and the light MSSM Higgs bosons rather difficult in the decoupling regime. For completeness, we have also analyzed the pair production of the heavy neutral Higgs particles of the MSSM. Up to phase space suppression factors, the cross sections for the processes

$$e^+e^- \rightarrow HH \text{ and } AA \quad (3)$$

are of the same order as the SM Higgs pair production cross section. In contrast, due to mixing angle factors suppression, the cross section for

$$e^+e^- \rightarrow Hh \quad (4)$$

is at least one order of magnitude smaller, but the supersymmetric contributions are of the same size as the  $W/Z$ /Higgs contributions. The processes  $e^+e^- \rightarrow HA/hA$  and  $e^+e^- \rightarrow H^+H^-$  appear already at the tree level, and will not be considered here<sup>2</sup>.

The rest of the paper is organised as follows. In the next section we present the cross sections for the Higgs pair production process in the Standard Model. In section 3, we discuss the case of the Higgs pair production process in the MSSM. Some conclusions will be drawn in section 4. In the Appendix, we will give the lengthy analytical expressions of the cross sections in the MSSM.

---

<sup>1</sup>This process is similar to the double Higgs production  $W^*W^* \rightarrow H^0H^0$  or  $e^+e^- \rightarrow ZH^0H^0 \rightarrow \nu\bar{\nu}H^0H^0$ , which consist of the same final state [although with missing energy] and which can be used to measure the trilinear Higgs self-coupling [6].

<sup>2</sup>The radiative corrections to these processes, including the contributions of the supersymmetric particles, have been recently discussed in Refs. [9, 10, 13].

## 2. SM Higgs Pair Production

In the Standard Model, many Feynman diagrams could in principle contribute to the amplitude for the Higgs boson pair production process, eq.(1). However, in the limit of vanishing electron mass, which implies a vanishing  $He$  coupling, the contributions of the tree-level diagrams where the Higgs bosons are emitted from the electron lines are negligible. Non-zero contributions to the process  $e^+e^- \rightarrow H^0H^0$  can therefore only come from one-loop diagrams.

Because of the exact chiral symmetry for  $m_e = 0$ , all diagrams involving the one-loop  $He^+e^-$  vertex must give zero contributions [in fact this statement is valid to all orders in perturbation theory]. Furthermore, because of CP invariance, the amplitudes of the diagrams with  $\gamma$  and  $Z$  boson  $s$ -channel exchanges, which give rise to two Higgs bosons through vertex diagrams, also vanish [the contribution of the longitudinal component of the  $Z$  boson will be proportional to the electron mass, and is therefore negligible]. Additional contributions from vertex diagrams involving the quartic  $WWH^0H^0/ZZH^0H^0$  couplings are proportional to the electron/neutrino masses and are again negligible. The only contribution to Higgs pair production in the Standard Model will therefore come from  $W$  and  $Z$  box diagrams, Fig.1a.

Working in the Feynman gauge, where the  $W/Z$  boson contributions can be split into the  $g_{\mu\nu}$  and the neutral Goldstone parts, the ultraviolet-finite amplitudes have been reduced from a complicated tensorial form to scalar Passarino-Veltman functions [14] using the package FORM [15]. Before the reduction to scalar functions, we have verified that our expressions agree with those obtained in Ref.[12]. The amplitudes have then been symmetrized and squared; a factor of  $1/2$  has been included because of the two identical particles in the final state. Allowing for the polarization of both the electron and positron beams, which are respectively denoted by  $\lambda_-$  and  $\lambda_+$ , the differential cross section of the process (1) [in the limit  $m_e = 0$ ] is then given by

$$\frac{d\sigma}{d\cos\theta} = \frac{G_F^4 M_W^8}{1024\pi^5} \frac{\sqrt{1-4M_H^2/s}}{s(u t - M_H^4)} \left\{ (1+\lambda_-)(1-\lambda_+) \left| F^W + \frac{(2s_W^2-1)^2}{2c_W^4} F^Z \right|^2 + (1-\lambda_-)(1+\lambda_+) 4 \frac{s_W^8}{c_W^8} \left| F^Z \right|^2 \right\} \quad (5)$$

with  $s, t$  and  $u$  the usual Mandelstam variables,  $\theta$  the angle between the initial electron and one of the Higgs bosons, and  $s_W^2 = 1 - c_W^2 = \sin^2\theta_W$ . The form factor  $F^V$  with  $V = W/Z$  can be split into two terms corresponding to the contributions of the  $g_{\mu\nu}$  and Goldstone parts

$$F^V = 2M_V^2 F_1^V + F_2^V \quad (6)$$

where, in terms of the scalar two, three and four-point Passarino-Veltman functions<sup>3</sup>,

---

<sup>3</sup>The complete analytical expressions of the scalar functions can be found in Ref.[16] for instance; for their numerical evaluation we have used the package FF [17].

denoted respectively by  $B_0, C_0$  and  $D_0$ , the form factors  $F_{1,2}^V$  are given by

$$\begin{aligned} F_1^V &= \left\{ \left[ 2M_H^2 u - M_V^2 (u-t) - u(u+t) \right] D_0 - s C_0 (M_V^2, 0, M_V^2, 0, 0, s) \right. \\ &\quad \left. + (M_H^2 - u) \left[ C_0 (M_V^2, 0, M_V^2, 0, u, M_H^2) + C_0 (0, M_V^2, M_V^2, 0, M_H^2, u) \right] \right. \\ &\quad \left. + (u-t) C_0 (M_V^2, M_V^2, M_V^2, s, M_H^2, M_H^2) \right\} + \left\{ t \longleftrightarrow u \right\} \end{aligned} \quad (7)$$

$$\begin{aligned} F_2^V &= \left\{ \left[ t u - u^2 + 2 u M_H^2 - 2 M_H^4 \right] C_0 (M_V^2, 0, M_V^2, 0, 0, s) \right. \\ &\quad + u (u - M_H^2) \left[ C_0 (M_V^2, 0, M_V^2, 0, u, M_H^2) + C_0 (0, M_V^2, M_V^2, 0, M_H^2, u) \right] \\ &\quad - \frac{t^2 u - u^2 t - 2u^3 + 4 M_H^2 (t u - u^2) + M_H^4 (t + u)}{2(s - 4 M_H^2)} C_0 (M_V^2, M_V^2, M_V^2, s, M_H^2, M_H^2) \\ &\quad + \left[ u^2 (u - t) + M_V^2 u (t + u) + 2 u M_H^2 (M_H^2 - u) - 2 M_H^4 M_V^2 \right] D_0 \\ &\quad \left. + \frac{u t - M_H^4}{s - 4 M_H^2} [B_0 (M_V^2, M_V^2, M_H^2) - B_0 (M_V^2, M_V^2, s)] \right\} + \left\{ t \longleftrightarrow u \right\} \end{aligned} \quad (8)$$

with

$$D_0 \equiv D_0 (M_V^2, 0, M_V^2, M_V^2, 0, 0, M_H^2, M_H^2, s, u) \quad (9)$$

The cross sections are shown in Fig.2a as a function of the Higgs boson mass for two center-of-mass energies,  $\sqrt{s} = 500$  GeV and 1.5 TeV. Except when approaching the  $2M_H$  threshold [and the small dip near the  $WW$  threshold], the cross sections are practically constant for a given value of the c.m. energy, and amount to  $\sigma \sim 0.2$  fb at  $\sqrt{s} = 500$  GeV in the unpolarized case. The decrease of the cross sections with increasing center-of-mass energy is very mild: at  $\sqrt{s} = 1.5$  TeV, the cross section is still at the level of  $\sigma \sim 0.15$  fb for Higgs boson masses less than  $M_H \lesssim 350$  GeV.

The effect of polarizing the initial electron/positron beams is also shown in Fig.2a. With left-handed polarized electrons, the cross section  $e_L^- e^+ \rightarrow H^0 H^0$  is larger by a factor of two, while for left-handed electrons and right-handed positrons, the cross section  $e_L^- e_R^+ \rightarrow H^0 H^0$  is larger by a factor of four, compared to the unpolarized case. [These simple factors of 2 and 4 are due to the fact that the contribution of the  $W$  boson is much more important than the one of the  $Z$  boson, a mere consequence of the larger charged current couplings compared to the neutral current couplings.] Therefore, the availability of longitudinal polarization of the initial beams is very important.

With integrated luminosities of the order of  $\int \mathcal{L} \sim 100$  fb $^{-1}$  which are expected to be available for future high-energy linear colliders, one could expect a few hundred events in the course of a few years, if both initial beams can be longitudinally polarized.

Fig.2b shows the angular distributions  $d\sigma/d\cos\theta$  at a center-of-mass energy of  $\sqrt{s} = 500$  GeV for a Higgs boson mass of  $M_H = 150$  GeV. It is forward-backward symmetric, a consequence of the two identical particles in the final state, and follows approximately the  $d\sigma/d\cos\theta \sim \sin^2\theta$  law. Again, the angular distribution does not strongly depend on the Higgs mass and on the c.m. energy, except near the  $2M_H$  production threshold.

For Higgs masses below  $M_H \lesssim 140$  GeV, the signal will mainly consist of four  $b$  quarks in the final state,

$$e^+e^- \rightarrow H^0H^0 \rightarrow b\bar{b} b\bar{b} \quad (10)$$

since the dominant decay mode of the SM Higgs boson in this mass range is  $H^0 \rightarrow b\bar{b}$ . This calls for very efficient  $\mu$ -vertex detectors to tag the  $b$  quark jets. Since these rare events will be searched for only after the discovery of the Higgs boson in the main production processes, the Higgs boson mass will be precisely known and the two mass constraints  $m(b\bar{b}) = M_H$ , together with the rather large number of  $b$  quarks in the final state, give a reasonable hope to experimentally isolate the signals despite of the low rates.

For larger Higgs masses,  $M_H \gtrsim 140$  GeV, since  $H^0 \rightarrow W^+W^-$  and  $H^0 \rightarrow ZZ$  will be the dominant decay modes of the Higgs boson, the signals will consist of four gauge bosons in the final state,

$$e^+e^- \rightarrow H^0H^0 \rightarrow W^+W^-W^+W^- , W^+W^-ZZ , ZZZZ \quad (11)$$

leading to eight final fermions. These rather spectacular events should also help to experimentally isolate the signal.

Although the discussion of the background events is beyond the scope of this paper, a few comments are nevertheless in order.

(i) For light Higgs bosons, assuming that  $b$  quarks will be efficiently tagged, the main backgrounds will consist of the QCD 4  $b$ -jet process,  $ZH^0$  and  $ZZ$  pair production with the  $Z$  bosons decaying into  $b\bar{b}$  pairs, the latter background being the most dangerous especially if  $M_H \sim M_Z$ . However, since  $ZZ$  production is mediated by  $t$ -channel electron exchange, the cross section is strongly peaked in the forward and backward directions contrary to the signal process as shown in Fig.2b; a strong cut on  $\cos\theta$  should considerably reduce the background, while leaving the signal almost unaltered.

(ii) For higher Higgs boson masses, multiple vector boson production will be the main background; however, since these are higher-order processes in the electroweak coupling, the cross sections should be small enough for this background to be manageable.

(iii) Finally, one should note that double Higgs production in  $WW$  fusion,  $e^+e^- \rightarrow H^0H^0\nu\bar{\nu}$  and in the bremsstrahlung process  $e^+e^- \rightarrow H^0H^0 + Z[\rightarrow \nu\bar{\nu}]$  would also act as backgrounds since the two neutrinos will escape undetected. However, the requirement of no missing energy in the final state will easily discard these events.

### 3. MSSM Higgs Pair Production

In the case of the pair production of the CP–even Higgs bosons of the Minimal Supersymmetric Standard Model,  $e^+e^- \rightarrow \Phi_1\Phi_2$  with  $\Phi_1, \Phi_2 \equiv h, H$ , several additional Feynman diagrams will contribute to the processes; Fig.1b. Besides the  $W$  and  $Z$  boson box diagrams, one first has the box diagrams with the exchange of the pseudoscalar and the charged Higgs bosons,  $A$  and  $H^\pm$ . Then, one has two classes of box diagrams built up by chargino/sneutrino and neutralino/selectron loops<sup>4</sup>. These two sets consist of diagrams where both Higgs bosons couple to the neutralino/chargino or to slepton pairs, and diagrams where one Higgs boson couples to neutralinos/charginos and the other to sleptons. One has also to include the crossed diagrams in Fig.1b, with the exchange of  $\Phi_1$  and  $\Phi_2$ .

For the pair production of the CP–odd Higgs boson in the MSSM,  $e^+e^- \rightarrow AA$ , only a small subset of the previous Feynman diagrams contributes; Fig.1c and the corresponding crossed diagrams. Indeed, because of CP invariance the pseudoscalar Higgs boson does not couple to vector boson pairs and to slepton pairs [in the latter case, the couplings would be proportional to the lepton masses,  $m_e$  and  $m_\nu$ ]. The only relevant contributions will therefore come from the diagrams with  $h, H, H^\pm$  boson exchange, and those with chargino/sneutrino and neutralino/selectron exchanges, where both  $A$  bosons are emitted from the neutralino/chargino lines.

We have calculated the cross sections of the four processes eqs.(2,3) and (4) in the MSSM, following the same steps as those discussed in the case of the SM Higgs pair production. The analytical expressions of the cross sections are much more involved than in the SM case, a consequence of the many additional contributions, and in the case of  $e^+e^- \rightarrow Hh$ , of the two different particles in the final state. These expressions will therefore be given in the Appendix. Here, we will simply describe our inputs and discuss the numerical results which have been obtained.

Besides the four masses  $M_h, M_H, M_A$  and  $M_{H^\pm}$  of the Higgs particles, two additional parameters determine the Higgs sector of the MSSM at the tree level: the ratio  $\tan\beta = v_2/v_1$  of the vacuum expectation values of the two Higgs doublet fields and a mixing angle  $\alpha$  in the neutral CP–even sector. However, supersymmetry leads to several relations among these parameters and only two of them are in fact independent: if the pseudoscalar Higgs mass  $M_A$  and  $\tan\beta$  are specified, all other masses and the mixing angle  $\alpha$  can be derived at the tree–level [1]. Supersymmetry imposes a strong hierarchical structure on the mass spectrum,  $M_h < M_A < M_H, M_W < M_{H^\pm}$  and  $M_h < M_Z$ , which however is broken by radiative corrections [18].

The leading part of the radiative corrections grows as the fourth power of the top quark mass  $m_t$  and the logarithm of the common squark mass  $M_S$  [18]. At the subleading level the radiative corrections will introduce the supersymmetric Higgs mass parameter  $\mu$  and the parameters  $A_t, A_b$  in the soft symmetry breaking interaction [19]. In our analysis,

---

<sup>4</sup>Vertex diagrams involving the quartic slepton–slepton– $\Phi_1$ – $\Phi_2$  couplings will give rise to contributions which are proportional to the mixing between the two slepton eigenstates. Since this mixing is proportional to the partner lepton masses  $m_e$  and  $m_\nu$ , these diagrams give negligible contributions.

we will take into account the full one-loop corrections for the Higgs boson masses [9]; for the mixing angle we will use the one-loop improved [20] relation [ $\tan \beta$  and  $M_A$  are the input parameters and  $M_h$  is the full one-loop corrected  $h$  boson mass]

$$\tan \alpha = \frac{-(M_A^2 + M_Z^2) \tan \beta}{M_Z^2 + M_A^2 \tan^2 \beta - (1 + \tan^2 \beta) M_h} \quad (12)$$

Once these parameters are fixed, the couplings of the Higgs particles to gauge bosons and fermions will also be uniquely fixed; the Higgs–vector boson couplings relevant to our analysis are given in Table 1a.

To fully describe the supersymmetric sector two parameters must be introduced, in addition to  $M_A, \tan \beta, M_S, A_t, A_b$  and  $\mu$ . These are the gaugino mass parameter  $M_2$  [we will use the GUT relation which fixes the bino mass in terms of the gaugino mass,  $M_1 = \frac{5}{3} \tan^2 \theta_W M_2$ ] and the common slepton mass  $M_L$ . The masses of the four neutralinos  $\chi_i^0$  [ $i = 1, \dots, 4$ ] and the two charginos  $\chi_i^+$  [ $i = 1, 2$ ] are then completely fixed by  $\tan \beta, \mu$  and  $M_2$ . The masses of the left– and right–handed selectron  $\tilde{e}_L, \tilde{e}_R$ , and of the left–handed electronic sneutrino  $\tilde{\nu}_L$  will be fixed by  $M_L$  [in practice these masses will approximately be given by  $m_{\tilde{e}_L} \simeq m_{\tilde{e}_R} \simeq m_{\tilde{\nu}_L} = M_L$ ; the mixing between the two selectron states is negligible].

For the couplings of the Higgs bosons to neutralinos, charginos and sleptons, one also will need the value of the mixing angle  $\alpha$  which is fixed by  $\tan \beta$  and  $M_A$ . These couplings are given in Tables 1b–1c; the couplings of the electrons to charginos/neutralinos and sleptons which will also be needed in the analysis are given in the Appendix.

We are now in a position to discuss the numerical results. The cross sections for the four processes  $e^+e^- \rightarrow hh, HH, AA$  and  $hH$  are displayed in Figs.3–6, as a function of the Higgs boson masses and for two values of the c.m. energy  $\sqrt{s} = 500$  GeV and 1.5 TeV [except for  $hH$  production] and two representative values of  $\tan \beta = 1.5$  and 50. In all the figures we have chosen the parameters  $M_2 = -\mu = 150$  GeV, while the common slepton and squark masses are taken to be  $M_L = 300$  GeV and  $M_S = 500$  GeV; the parameter  $A_t$  and  $A_b$  are set to zero. Only the unpolarized cross sections are discussed: as mentioned previously, they are simply increased by a factor of 2(4) when the initial beam(s) are longitudinally polarized.

Fig.3 shows the cross section for the process  $e^+e^- \rightarrow hh$ . The solid lines are for the full cross sections, while the dashed lines are for the cross sections without the SUSY contributions [this will correspond to a two–Higgs doublet model with the MSSM constraints]. Let us first discuss the case where the supersymmetric contributions are not included. For small  $\tan \beta$ , the cross section is of the same order as the SM cross section and does not strongly depend on  $M_h$  especially at very high–energies. Although the  $WWh/Zhh$  couplings are suppressed by  $\sin(\beta - \alpha)$  factors, the suppression is not very strong and the  $W/Z$  box contributions are not much smaller than in the SM; the diagrams where  $A/H^\pm$  are exchanged will give compensating contributions since the  $hAZ/hH^\pm W$  couplings are proportional to the complementary factor  $\cos(\beta - \alpha)$ . As in the SM case, the cross sections

slightly decrease with increasing energy.

For large  $\tan\beta$  values, the factors  $\sin / \cos(\beta - \alpha)$  vary widely when  $M_h$  is varied. For small  $M_h$ , the factor  $\sin(\beta - \alpha) \rightarrow 0$ , and the contribution of the diagrams with  $A/H^\pm$  exchange dominates. The latter contribution decreases with increasing  $M_h$  [i.e. with decreasing  $\cos(\beta - \alpha)$ ], until the decoupling limit is reached for  $M_h \simeq 110$  GeV. In this case, the factor  $\sin(\beta - \alpha) \rightarrow 1$  and the  $W/Z$  boson loops are not suppressed anymore; one then obtains the SM cross section.

The contributions of the chargino/selectron and neutralino/sneutrino loops lead to a destructive interference. At high–energies, the supersymmetric boxes practically do not contribute; but at low energies, and especially below the decoupling limit, the SUSY contributions can be of the order of  $\sim 10\%$ . We have scanned the SUSY parameter space, and the maximum contribution of the SUSY loops that we have found was about  $\sim -15\%$ . In the decoupling limit, the SUSY contributions are, at most, of the order of a few percent. Because of the rather low production rates, it will therefore be difficult to experimentally see this effect.

Fig.4 and 5 show the cross sections for the processes  $e^+e^- \rightarrow HH$  and  $e^+e^- \rightarrow AA$ , respectively. Except for small  $A/H$  masses where they are of the same order as in the SM, the cross sections are below the 0.1 fb level and the signals will be hard to detect, especially for  $M_A, M_H \gtrsim 350$  GeV [independently of the phase space suppression]. The SUSY contributions are relatively even smaller than for the case of  $e^+e^- \rightarrow hh$ .

Finally, Fig.6 shows the cross section for the case  $e^+e^- \rightarrow hH$  at  $\sqrt{s} = 500$  GeV. It is one order of magnitude smaller than in the previous cases and therefore negligibly small. This is due to the fact that the  $W/Z$  and  $A/H^\pm$  contributions are both suppressed since the combination  $\sin(\beta - \alpha) \times \cos(\beta - \alpha)$  appears in all these contributions; since one of the factors is always small, this brings these contributions down to the level of the small SUSY–loop contributions.

## 4. Summary

We have analyzed the one–loop induced production of Higgs boson pairs at future high–energy  $e^+e^-$  colliders in the Standard Model and in the Minimal Supersymmetric Standard Model. In the SM, the unpolarized cross section is rather small, of the order 0.1–0.2 fb. The longitudinal polarization of both the  $e^-$  and  $e^+$  beams will increase the cross section by a factor of 4. With integrated luminosities  $\int \mathcal{L} \gtrsim 100$  fb $^{-1}$  as expected to be the case for future high–energy linear colliders, one could expect a few hundred events in the course of a few years if longitudinal polarization is available. The final states are rather clean, giving a reasonable hope to isolate the signals experimentally.

In the MSSM, additional contributions to the processes  $e^+e^- \rightarrow hh, HH, Hh$  and  $e^+e^- \rightarrow AA$  come from chargino/neutralino and slepton loops. For  $hh$  production, the contributions of the supersymmetric loops are in general rather small, being of the order of a few percent; the cross sections are therefore of the same order as in the SM. For

the processes involving heavy Higgs bosons, the cross sections are even smaller than for  $e^+e^- \rightarrow hh$ , and the signals will be hard to be detected experimentally.

**Acknowledgements:** We thank W. Hollik for discussions and J. Rosiek for providing us with the Fortran code for the one-loop corrected MSSM Higgs boson masses.

## APPENDIX: Cross sections in the MSSM

In this Appendix, we will give the analytical expressions of the cross sections for the pair production of the MSSM Higgs bosons. We start with the production of two CP-even Higgs bosons,  $e^+e^- \rightarrow \Phi_1\Phi_2$  with  $\Phi_1, \Phi_2 \equiv h, H$ . Similarly to the SM case, the differential cross section for the process can be written as:

$$\frac{d\sigma}{d\cos\theta} = \frac{1}{1 + \delta_{\Phi_1\Phi_2}} \frac{G_F^4 M_W^8}{8\pi^5 s} \left[ \left( 1 - \frac{M_{\Phi_1}^2}{s} - \frac{M_{\Phi_2}^2}{s} \right)^2 - 4 \frac{M_{\Phi_1}^2 M_{\Phi_2}^2}{s^2} \right]^{1/2} (ut - M_{\Phi_2}^2 M_{\Phi_1}^2) \left[ (1 + \lambda_-)(1 - \lambda_+) \left| \sum_{k=1}^9 F_k^+ \right|^2 + (1 - \lambda_-)(1 + \lambda_+) \left| \sum_{k=1}^9 F_k^- \right|^2 \right] \quad (\text{A1})$$

where  $\lambda_-$  and  $\lambda_+$  are the longitudinal polarizations of the initial  $e^-$  and  $e^+$  beams,  $\theta$  the scattering angle and  $s, t, u$  the usual Mandelstam variables;  $\delta_{\Phi_1\Phi_2} = 1$  in the case where we have two identical Higgs bosons in the final state, otherwise  $\delta_{\Phi_1\Phi_2} = 0$ .

For the class of diagrams consisting of  $W/Z$  and  $A/H^\pm$  loops [a two Higgs-doublet model], there are three contributing amplitudes  $F_{1,2,3}^\pm$  given by

$$\begin{aligned} F_1^+ &= g_{\Phi_1 VV} g_{\Phi_2 VV} \frac{M_W^2}{2} \left[ \frac{(2s_W^2 - 1)^2}{2c_W^6} F_A(M_Z, 0, M_Z, M_Z, s, t) + F_A(M_W, 0, M_W, M_W, s, t) \right] \\ F_1^- &= g_{\Phi_1 VV} g_{\Phi_2 VV} \frac{M_Z^2 s_W^4}{c_W^4} F_A(M_Z, 0, M_Z, M_Z, s, t) \\ F_2^+ &= g_{\Phi_1 VV} g_{\Phi_2 VV} \left[ \frac{(2s_W^2 - 1)^2}{16 c_W^4} F_B(M_Z, 0, M_Z, M_Z, s, t) + \frac{1}{8} F_B(M_W, 0, M_W, M_W, s, t) \right] \\ F_2^- &= g_{\Phi_1 VV} g_{\Phi_2 VV} \frac{s_W^4}{4 c_W^4} F_B(M_Z, 0, M_Z, M_Z, s, t) \\ F_3^+ &= g_{\Phi_1 AV} g_{\Phi_2 AV} \frac{(2s_W^2 - 1)^2}{16 c_W^4} F_B(M_Z, 0, M_Z, M_A, s, t) \\ &\quad + g_{\Phi_1 H^\pm W^\pm} g_{\Phi_2 H^\pm W^\pm} \frac{1}{8} F_B(M_W, 0, M_W, M_{H^\pm}, s, t) \\ F_3^- &= g_{\Phi_1 AV} g_{\Phi_2 AV} \frac{s_W^4}{4 c_W^4} F_B(M_Z, 0, M_Z, M_A, s, t) \end{aligned} \quad (\text{A2})$$

where the couplings  $g_{\Phi VV}$ ,  $g_{\Phi AZ}$  and  $g_{\Phi H^\pm W}$  are given in Table 1a. In terms of the  $D_{ijk}$  four-point Passarino–Veltman functions [14], the form factors  $F_{A,B} \equiv F_{A,B}(m_1, m_2, m_3, m_4, s, t)$  [the analogous of  $F_1$  and  $F_2$  of eqs.(7) and (8)] are given by

$$F_A = D_{13} + \{u \leftrightarrow t, M_{\Phi_1} \leftrightarrow M_{\Phi_2}\} \quad (\text{A3})$$

$$\begin{aligned} F_B = & \left[ 2(M_{\Phi_2}^2 - u) D_0 + 2(M_{\Phi_2}^2 - u) D_{11} + 2(M_{\Phi_2}^2 - t) D_{12} + 2t D_{13} \right. \\ & + \frac{3M_{\Phi_1}^2 + t}{2} D_{23} + 2s D_{24} + 2(t - M_{\Phi_1}^2) D_{25} + \frac{s + 4(u - M_{\Phi_1}^2)}{2} D_{26} + 8 D_{27} \\ & + \frac{M_{\Phi_1}^2}{2} D_{33} + \frac{t - M_{\Phi_1}^2}{2} D_{37} + \frac{u - M_{\Phi_1}^2}{2} D_{39} + \frac{s}{2} D_{310} + 3 D_{313} \Big] \\ & + \{u \leftrightarrow t, M_{\Phi_1} \leftrightarrow M_{\Phi_2}\} \end{aligned} \quad (\text{A4})$$

with

$$D_{ijk} \equiv D_{ijk}(m_1, m_2, m_3, m_4, 0, 0, M_{\Phi_1}, M_{\Phi_2}, s, t)$$

For the class of diagrams consisting of sneutrino/chargino loops, the contributing amplitudes  $F_{4,5,6}^\pm$  are given by

$$\begin{aligned} F_4^+ = & - \sum_{i=1}^2 \frac{M_Z^2}{8 c_W^2} g_{e\chi_i^+\tilde{\nu}} g_{e\chi_i^+\tilde{\nu}} g_{\Phi_1\tilde{\nu}\tilde{\nu}} g_{\Phi_2\tilde{\nu}\tilde{\nu}} F_A(m_{\tilde{\nu}}, -m_{\chi_i^+}, m_{\tilde{\nu}}, m_{\tilde{\nu}}, s, t) \\ F_5^+ = & \sum_{i,j=1}^2 \frac{M_Z}{2 c_W} g_{e\chi_i^+\tilde{\nu}} g_{e\chi_j^+\tilde{\nu}} \\ & \sum_{a=L,R} \left[ g_{\Phi_1\tilde{\nu}\tilde{\nu}} g_{\Phi_2\chi_i^+\chi_j^-}^a F_C^{+a}(-m_{\chi_i^+}, m_{\tilde{\nu}}, m_{\tilde{\nu}}, -m_{\chi_j^+}, s, t, M_{\Phi_1}, M_{\Phi_2}) \right. \\ & \left. + g_{\Phi_2\tilde{\nu}\tilde{\nu}} g_{\Phi_1\chi_i^+\chi_j^-}^a F_C^{+a}(-m_{\chi_i^+}, m_{\tilde{\nu}}, m_{\tilde{\nu}}, -m_{\chi_j^+}, s, u, M_{\Phi_2}, M_{\Phi_1}) \right] \\ F_6^+ = & - \sum_{i,j,k=1}^2 g_{e\chi_i^+\tilde{\nu}} g_{e\chi_k^+\tilde{\nu}} \\ & \sum_{a,b=L,R} \left[ g_{\Phi_1\chi_i^+\chi_j^-}^a g_{\Phi_2\chi_j^+\chi_k^-}^b F_D^{+ab}(-m_{\chi_i^+}, m_{\tilde{\nu}}, -m_{\chi_k^+}, -m_{\chi_j^+}, s, t, M_{\Phi_1}, M_{\Phi_2}) \right. \\ & \left. + g_{\Phi_2\chi_i^+\chi_j^-}^a g_{\Phi_1\chi_j^+\chi_k^-}^b F_D^{+ab}(-m_{\chi_i^+}, m_{\tilde{\nu}}, -m_{\chi_k^+}, -m_{\chi_j^+}, s, u, M_{\Phi_2}, M_{\Phi_1}) \right] \end{aligned} \quad (\text{A5})$$

and

$$F_{4,5,6}^- = 0 \quad (\text{A6})$$

$F_A$  is given in eq.(A3), and the new form factors  $F_C^{\pm a} \equiv F_C^{\pm a}(m_1, m_2, m_3, m_4, s, t, M_{\Phi_1}, M_{\Phi_2})$  and  $F_D^{\pm ab} \equiv F_D^{\pm ab}(m_1, m_2, m_3, m_4, s, t, M_{\Phi_1}, M_{\Phi_2})$ , with  $a, b = L, R$ , are given by

$$F_C^{-R} = F_C^{+L} = \frac{1}{2} (m_1 D_0 + m_1 D_{12})$$

$$\begin{aligned}
F_C^{-L} &= F_C^{+R} &= \frac{1}{2} m_4 D_{12} \\
F_D^{-RR} &= F_D^{+LL} &= -\frac{1}{2} m_1 m_4 D_{13} \\
F_D^{-RL} &= F_D^{+LR} &= \frac{1}{2} \left[ s(D_{12} + D_{13}) + (s - M_{\Phi_2}^2) D_{23} + s(D_{24} - D_{25} - D_{26}) + 2 D_{27} \right. \\
&\quad \left. - M_{\Phi_1}^2 D_{33} - (t - M_{\Phi_1}^2) D_{37} - (u - M_{\Phi_1}^2) D_{39} - s D_{310} - 6 D_{313} \right] \\
F_D^{-LR} &= F_D^{+RL} &= -\frac{1}{2} m_1 m_3 (D_0 + D_{13}) \\
F_D^{-LL} &= F_D^{+RR} &= -\frac{1}{2} m_3 m_4 D_{13}
\end{aligned} \tag{A7}$$

Finally, for the class of diagrams consisting of selectron/neutralino loops, the amplitudes  $F_{7,8,9}^\pm$  are given by

$$\begin{aligned}
F_7^+ &= \sum_{i=1}^4 \frac{M_Z^2}{8 c_W^2} g_{e\chi_i^0 \tilde{e}_R} g_{e\chi_i^0 \tilde{e}_R} g_{\Phi_1 \tilde{e}_R \tilde{e}_R} g_{\Phi_2 \tilde{e}_R \tilde{e}_R} F_A(m_{\tilde{e}_R}, m_{\chi_i^0}, m_{\tilde{e}_R}, m_{\tilde{e}_R}, s, t) \\
F_8^+ &= \sum_{i,j=1}^4 \frac{M_Z}{4 c_W} g_{e\chi_i^0 \tilde{e}_R} g_{e\chi_j^0 \tilde{e}_R} \\
&\quad \sum_{a=L,R} \left[ g_{\Phi_1 \tilde{e}_R \tilde{e}_R} g_{\Phi_2 \chi_i^0 \chi_j^0} F_C^{+a}(m_{\chi_i^0}, m_{\tilde{e}_R}, m_{\tilde{e}_R}, m_{\chi_j^0}, s, t, M_{\Phi_1}, M_{\Phi_2}) \right. \\
&\quad \left. + g_{\Phi_2 \tilde{e}_R \tilde{e}_R} g_{\Phi_1 \chi_i^0 \chi_j^0} F_C^{+a}(m_{\chi_i^0}, m_{\tilde{e}_R}, m_{\tilde{e}_R}, m_{\chi_j^0}, s, u, M_{\Phi_2}, M_{\Phi_1}) \right] \\
F_9^+ &= \sum_{i,j,k=1}^4 \frac{1}{2} g_{e\chi_i^0 \tilde{e}_R} g_{e\chi_k^0 \tilde{e}_R} \\
&\quad \sum_{a,b=L,R} \left[ g_{\Phi_1 \chi_i^0 \chi_j^0}^a g_{\Phi_2 \chi_j^0 \chi_k^0}^b F_D^{+ab}(m_{\chi_i^0}, m_{\tilde{e}_R}, m_{\chi_k^0}, m_{\chi_j^0}, s, t, M_{\Phi_1}, M_{\Phi_2}) \right. \\
&\quad \left. + g_{\Phi_2 \chi_i^0 \chi_j^0}^a g_{\Phi_1 \chi_j^0 \chi_k^0}^b F_D^{+ab}(m_{\chi_i^0}, m_{\tilde{e}_R}, m_{\chi_k^0}, m_{\chi_j^0}, s, u, M_{\Phi_2}, M_{\Phi_1}) \right]
\end{aligned} \tag{A8}$$

and

$$F_{7,8,9}^- = F_{7,8,9}^+ (\tilde{e}_R \rightarrow \tilde{e}_L, F_{C,D}^{+ab} \rightarrow F_{C,D}^{-ab}) \tag{A9}$$

where the form factors  $F_{A,B,C,D}$  have been given previously. The normalized couplings of the neutral Higgs bosons to charginos, neutralinos and sleptons are displayed in Tab. 1b and 1c. The only remaining couplings which have to be defined, are the electron–chargino–sneutrino and electron–neutralino–selectron couplings, which, normalized to  $g_W = [\sqrt{2}G_F]^{1/2} M_W$ , are given by

$$g_{e\chi_i^+ \tilde{\nu}} = V_{i1} \quad , \quad g_{e\chi_i^0 \tilde{e}_R} = -2 \frac{s_W}{c_W} N_{i2} \quad , \quad g_{e\chi_i^0 \tilde{e}_L} = -N_{i2} - \frac{s_W}{c_W} N_{i1} \tag{A10}$$

where the matrices  $V$  and  $N$  can be found in Ref.[21].

For the pair production of the CP-odd Higgs boson in the MSSM,  $e^+e^- \rightarrow AA$ , the differential cross section takes the form

$$\frac{d\sigma}{d\cos\theta} = \frac{G_F^4 M_W^8}{16 s \pi^5} \sqrt{1 - 4 \frac{M_A^2}{s}} (ut - M_A^4) \left[ (1 + \lambda_-)(1 - \lambda_+) \left| \sum_{k=10}^{12} F_k^+ \right|^2 + (1 - \lambda_-)(1 + \lambda_+) \left| \sum_{k=10}^{12} F_k^- \right|^2 \right] \quad (\text{A11})$$

where we have used the same notation as previously. The three contributing amplitudes  $F_{10,11,12}^\pm$  are given by

$$\begin{aligned} F_{10}^+ &= \frac{(2s_W^2 - 1)^2}{16 c_W^4} \left[ g_{hAV}^2 F_B(M_Z, 0, M_Z, M_h, s, t) \right. \\ &\quad \left. + g_{HAV}^2 F_B(M_Z, 0, M_Z, M_H, s, t) \right] + \frac{1}{8} g_{H^\pm AW}^2 F_B(M_W, 0, M_W, M_{H^\pm}, s, t) \\ F_{10}^- &= \frac{s_W^4}{4 c_W^4} \left[ g_{hAV}^2 F_B(M_Z, 0, M_Z, M_h, s, t) + g_{HAV}^2 F_B(M_Z, 0, M_Z, M_H, s, t) \right] \\ F_{11}^+ &= \sum_{i,j,k=1}^4 \frac{1}{2} g_{e\chi_i^0 \tilde{e}_R} g_{e\chi_k^0 \tilde{e}_R} \\ &\quad \sum_{a,b=L,R} \left[ g_{A\chi_i^0 \chi_j^0}^a g_{A\chi_j^0 \chi_k^0}^b F_D^{+ab}(m_{\chi_i^0}, m_{\tilde{e}_R}, m_{\chi_k^0}, m_{\chi_j^0}, s, t, M_A, M_A) \right. \\ &\quad \left. + g_{A\chi_i^0 \chi_j^0}^a g_{A\chi_j^0 \chi_k^0}^b F_D^{+ab}(m_{\chi_i^0}, m_{\tilde{e}_R}, m_{\chi_k^0}, m_{\chi_j^0}, s, u, M_A, M_A) \right] \\ F_{11}^- &= \sum_{i,j,k=1}^4 \frac{1}{2} g_{e\chi_i^0 \tilde{e}_L} g_{e\chi_k^0 \tilde{e}_L} \\ &\quad \sum_{a,b=L,R} \left[ g_{A\chi_i^0 \chi_j^0}^a g_{A\chi_j^0 \chi_k^0}^b F_D^{-ab}(m_{\chi_i^0}, m_{\tilde{e}_L}, m_{\chi_k^0}, m_{\chi_j^0}, s, t, M_A, M_A) \right. \\ &\quad \left. + g_{A\chi_i^0 \chi_j^0}^a g_{A\chi_j^0 \chi_k^0}^b F_D^{-ab}(m_{\chi_i^0}, m_{\tilde{e}_L}, m_{\chi_k^0}, m_{\chi_j^0}, s, u, M_A, M_A) \right] \\ F_{12}^+ &= - \sum_{i,j,k=1}^2 g_{e\chi_i^+ \tilde{\nu}} g_{e\chi_k^+ \tilde{\nu}} \\ &\quad \sum_{a,b=L,R} \left[ g_{A\chi_i^+ \chi_j^-}^a g_{A\chi_j^+ \chi_k^-}^b F_D^{+ab}(-m_{\chi_i^+}, m_{\tilde{\nu}}, -m_{\chi_k^+}, -m_{\chi_j^+}, s, t, M_A, M_A) \right. \\ &\quad \left. + g_{A\chi_i^+ \chi_j^-}^a g_{A\chi_j^+ \chi_k^-}^b F_D^{+ab}(-m_{\chi_i^+}, m_{\tilde{\nu}}, -m_{\chi_k^+}, -m_{\chi_j^+}, s, u, M_A, M_A) \right] \\ F_{12}^- &= 0 \end{aligned} \quad (\text{A12})$$

with  $F_B$  and  $F_D$  as given previously; the couplings of the pseudoscalar Higgs bosons to the neutralino and chargino states are again given in Table 1c.

## References

- [1] For a review on the Higgs sector of the SM and the MSSM , see J. Gunion, H. Haber, G. Kane and S. Dawson, *The Higgs Hunter's Guide*, Addison–Wesley, Reading 1990.
- [2] For recent discussions of Higgs physics at  $e^+e^-$  colliders, see the Proceedings,  *$e^+e^-$  collisions at 500 GeV: The Physics Potential*, Munich–Annecy–Hamburg, DESY 92–123A+C, P.M. Zerwas (ed.);  
A. Djouadi, *Int. J. Mod. Phys. A*10 (1995) 1.
- [3] J. Ellis, M.K. Gaillard and D.V. Nanopoulos, *Nucl. Phys.* B106 (1976) 292;  
B.W. Lee, C. Quigg and H.H. Thacker, *Phys. Rev. D*16 (1977) 1519;  
J.D. Bjorken, *Proc. Summer Inst. on Particle Physics*, SLAC Report 198 (1976);  
B. Ioffe and V.A. Khoze, *Sov. J. Part. Nucl.* 9, (1978) 50.
- [4] D.R.T. Jones and S.T. Petcov, *Phys. Lett.* B84 (1979) 440;  
R.N. Cahn and S. Dawson, *Phys. Lett.* B136 (1984) 196;  
K. Hikasa, *Phys. Lett.* B164 (1985) 341;  
G. Altarelli, B. Mele and F. Pitolli, *Nucl. Phys.* B287 (1987) 205.
- [5] K. Hagiwara, H. Murayama and I. Watanabe, *Nucl. Phys.* B367 (1991) 257;  
M. Hildreth, T.L. Barklow and D.L. Burke, *Phys. Rev. D*49 (1994) 3441.
- [6] G. Gounaris, D. Schildknecht and F. Renard, *Phys. Lett.* B83 (1979) 191 and Erratum 89B (1980) 437;  
V. Barger and T. Han, *Mod. Phys. Lett. A*5 (1990) 667;  
H. E. V. Ilyin et al., Report KEK CP–030;  
F. Boudjema and E. Chopin, ENSLAPP–A534/95;  
A. Djouadi, Haber and P. M. Zerwas, DESY–95–214 (hep-ph 9602234);  
J. Kamoshita, Y. Okada, M. Tanaka and I. Watanabe, Report KEK–TH–467.
- [7] A. Djouadi, J. Kalinowski and P. M. Zerwas, *Z. Phys. C*54 (1992) 255.
- [8] H.E. Haber, CERN-TH/95-109 and SCIPP-95/15, Proceedings, *Conference on Physics Beyond the Standard Model IV*, Lake Tahoe CA 1994; and *Perspectives for Electroweak Interactions in  $e^+e^-$  Collisions*, Ringberg Castle, Tegernsee 1995.
- [9] P. Chankowski, S. Pokorski and J. Rosiek, *Nucl. Phys. B* 423 (1994) 437; *Nucl. Phys. B*423 (1994) 497.
- [10] V. Driesen and W. Hollik, *Z. Phys. C* 68 (1995) 485;  
V. Driesen, W. Hollik and J. Rosiek, KA-TP-16-1995, hep-ph/9512441.
- [11] For recent discussions of the Higgs– $\gamma\gamma$  coupling in the MSSM see:  
G.L. Kane, G.D. Kribs, S.P. Martin and J.D. Wells, *Phys. Rev. D*53 (1996) 213;  
B. Kileng, P. Osland and P.N. Pandita, NORDITA-95-48-P (1995).

- [12] K. Gaemers and F. Hoogeveen, Z. Phys. C26 (1984) 249.
- [13] A. Arhrib, M. Capdequi-Peyranere and G. Mourtaka, Phys. Lett. B341 (1995) 313.
- [14] G. Passarino and M. Veltman, Nucl. Phys. B160 (1979) 151.
- [15] J.A.M. Vermaseren, *Symbolic manipulations with FORM*, 1991, CAN ed;  
G.J. Oldenborgh and J.A.M. Vermaseren, Z. Phys. C46 (1990) 425.
- [16] G. 't Hooft and M. Veltman, Nucl. Phys. B153 (1979) 365;  
A. Denner, Fortschr. Phys. 41 (1993) 4.
- [17] G.J. Oldenborgh, Comput. Phys. Comm. 66 (1991) 1.
- [18] H. Haber and R. Hempfling, Phys. Rev. Lett. 66 (1991) 1815;  
Y. Okada, M. Yamaguchi and T. Yanagida, Prog. Theor. Phys. 85 (1991) 1;  
J. Ellis, G. Ridolfi and F. Zwirner, Phys. Lett. 257B (1991) 83;  
R. Barbieri, F. Caravaglios and M. Figeni, Phys. Lett. 258B (1991) 167;  
R. Hempfling and A. Hoang, Phys. Lett. B331 (1994) 99;  
J. Casas, J. Espinosa, M. Quiros and A. Riotto, Nucl. Phys. B436 (1995) 3.
- [19] M. Carena, J. Espinosa, M. Quiros and C. Wagner, Phys. Lett. B355 (1995) 209.
- [20] A. Dabelstein, W. Hollik, MPI-PH/93-86, Nov 1993, Contribution to the Workshop  
 *$e^+e^-$  Collisions at 500 GeV: the Physics Potential*, DESY 92-123C;  
A. Dabelstein, Z. Phys. C 67 (1995) 495.
- [21] H.E. Haber and G. Kane, Phys. Rep. C 117 (1985) 75.

**Table 1:**

$\Phi$	$g_{\Phi VV}$	$g_{\Phi AZ}$	$g_{\Phi H^\pm W^\pm}$
$h$	$\sin(\beta - \alpha)$	$\cos(\beta - \alpha)$	$\mp \cos(\beta - \alpha)$
$H$	$\cos(\beta - \alpha)$	$-\sin(\beta - \alpha)$	$\pm \sin(\beta - \alpha)$
$A$	0	0	1

**Tab. 1a:** The Higgs–vector boson couplings  $g_{\Phi VV}$  [normalized the SM Higgs coupling  $g_{H^0 VV} = 2 \left[ \sqrt{2} G_F \right]^{1/2} M_V^2$ ], and the Higgs–Higgs–vector boson couplings [normalized to  $g_W = (\sqrt{2} G_F)^{1/2} M_W$  and  $g_Z = (\sqrt{2} G_F)^{1/2} M_Z$  for the charged/neutral weak couplings]; the latter come with the sum of the Higgs momenta entering and leaving the vertices.

$\tilde{l}_i \tilde{l}_j$	$g_{h \tilde{l}_i \tilde{l}_j}$	$g_{H \tilde{l}_i \tilde{l}_j}$	$g_{A \tilde{l}_i \tilde{l}_j}$
$\tilde{e}_L \tilde{e}_L$	$(2s_W^2 - 1) \sin(\beta + \alpha)$	$-(2s_W^2 - 1) \cos(\beta + \alpha)$	0
$\tilde{e}_R \tilde{e}_R$	$2s_W^2 \sin(\beta + \alpha)$	$-2s_W^2 \cos(\beta + \alpha)$	0
$\tilde{\nu}_L \tilde{\nu}_L$	$\sin(\beta + \alpha)$	$-\cos(\beta + \alpha)$	0

**Tab. 1b:** The couplings of the neutral Higgs bosons to left– and right–handed sleptons, normalized to  $g'_W = \left[ \sqrt{2} G_F \right]^{1/2} M_W^2$ .

$g^{L,R} / \Phi$	$h$	$H$	$A$
$g_{\Phi \chi_i^+ \chi_j^-}^L$ $g_{\Phi \chi_i^+ \chi_j^-}^R$	$Q_{ji}^* \sin \alpha - S_{ji}^* \cos \alpha$ $Q_{ij} \sin \alpha - S_{ij} \cos \alpha$	$-Q_{ji}^* \cos \alpha - S_{ji}^* \sin \alpha$ $-Q_{ij} \cos \alpha - S_{ij} \sin \alpha$	$-Q_{ji}^* \sin \beta - S_{ji}^* \cos \beta$ $Q_{ij} \sin \beta + S_{ij} \cos \beta$
$g_{\Phi \chi_i^0 \chi_j^0}^L$ $g_{\Phi \chi_i^0 \chi_j^0}^R$	$Q_{ji}^{''*} \sin \alpha + S_{ji}^{''*} \cos \alpha$ $Q_{ij}^{''} \sin \alpha + S_{ij}^{''} \cos \alpha$	$-Q_{ji}^{''*} \cos \alpha + S_{ji}^{''*} \sin \alpha$ $-Q_{ij}^{''} \cos \alpha + S_{ij}^{''} \sin \alpha$	$-Q_{ji}^{''*} \sin \beta + S_{ji}^{''*} \cos \beta$ $Q_{ij}^{''} \sin \beta - S_{ij}^{''} \cos \beta$

**Tab. 1c:** The couplings of the neutral Higgs bosons to charginos and neutralinos, normalized to  $g_W = \left[ \sqrt{2} G_F \right]^{1/2} M_W$ ; the matrix elements  $Q_{ij}/S_{ij}$  and  $Q_{ij}^{''}/S_{ij}^{''}$  can be found in Ref. [21].

## Figure Captions

**Fig. 1:** Feynman diagrams contributing to the Higgs boson pair production process in  $e^+e^-$  collisions: (a) SM Higgs production, CP-even (b) and CP-odd (c) Higgs boson production in the MSSM.

**Fig. 2:** a) The cross sections for the Higgs pair production in the SM,  $e^+e^- \rightarrow H^0H^0$ , as a function of the Higgs mass for two center-of-mass energies,  $\sqrt{s} = 500$  GeV [dashed lines] and  $\sqrt{s} = 1.5$  TeV [solid lines]. The lower curves correspond to the unpolarized cross sections, the middle curves to the cross sections where the electron beam is longitudinally polarized and the upper curves to the cross sections where both the electron and positron beams are longitudinally polarized. (b) The angular distribution as a function of the scattering angle in the unpolarized case, at  $\sqrt{s} = 500$  GeV and for  $M_H = 150$  GeV.

**Fig. 3:** The cross sections for the pair production of the lightest Higgs boson in the MSSM,  $e^+e^- \rightarrow hh$ , as a function of  $M_h$  for two center-of-mass energies,  $\sqrt{s} = 500$  GeV and  $\sqrt{s} = 1.5$  TeV and for two values of  $\tan\beta = 1.5$  and 50. The solid curves correspond to the full cross sections, while the dashed curves correspond to the cross sections without the SUSY contributions.

**Fig. 4:** The cross sections for the process  $e^+e^- \rightarrow HH$ , as a function of  $M_H$  for two center-of-mass energies,  $\sqrt{s} = 500$  GeV and  $\sqrt{s} = 1.5$  TeV and for two values of  $\tan\beta = 1.5$  and 50. The solid curves correspond to the full cross sections, while the dashed curves correspond to the cross sections without the SUSY contributions.

**Fig. 5:** The cross sections for the process  $e^+e^- \rightarrow AA$ , as a function of  $M_A$  for two center-of-mass energies,  $\sqrt{s} = 500$  GeV and  $\sqrt{s} = 1.5$  TeV and for two values of  $\tan\beta = 1.5$  and 50. The solid curves correspond to the full cross sections, while the dashed curves correspond to the cross sections without the SUSY contributions.

**Fig. 6:** The cross sections for the process  $e^+e^- \rightarrow Hh$ , as a function of  $M_H$  for  $\sqrt{s} = 500$  GeV and for two values of  $\tan\beta = 1.5$  and 50. The solid curves correspond to the full cross sections, while the dashed curves correspond to the cross sections without the SUSY contributions.

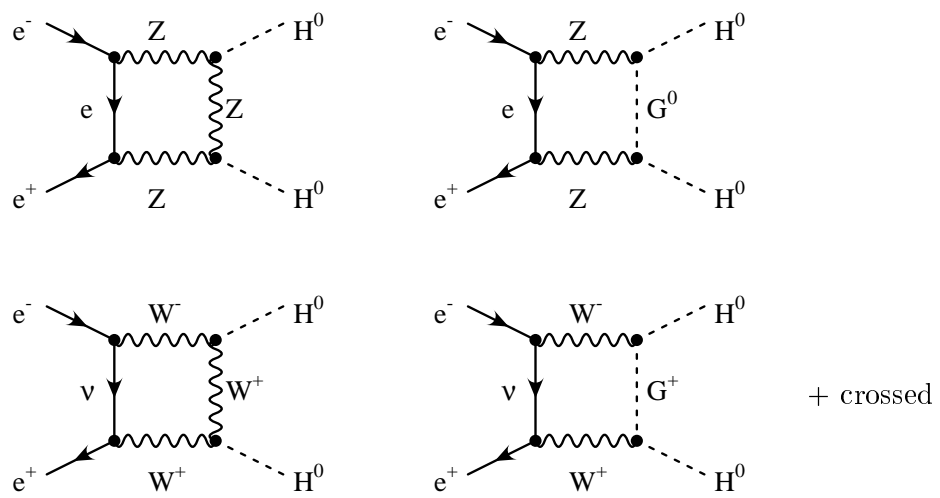


Fig. 1a

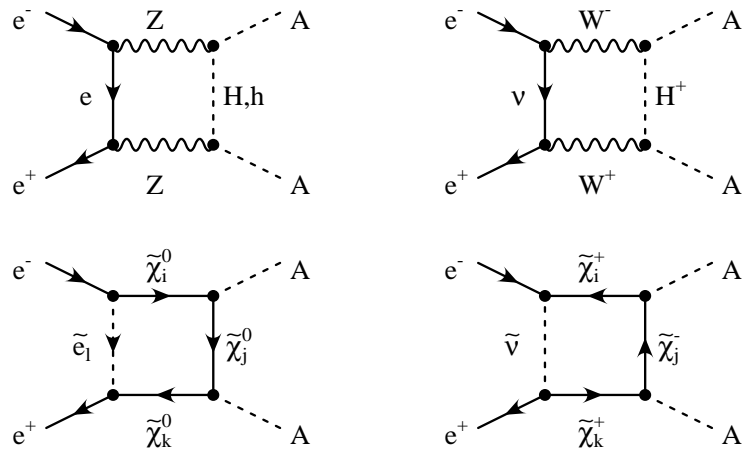


Fig. 1c

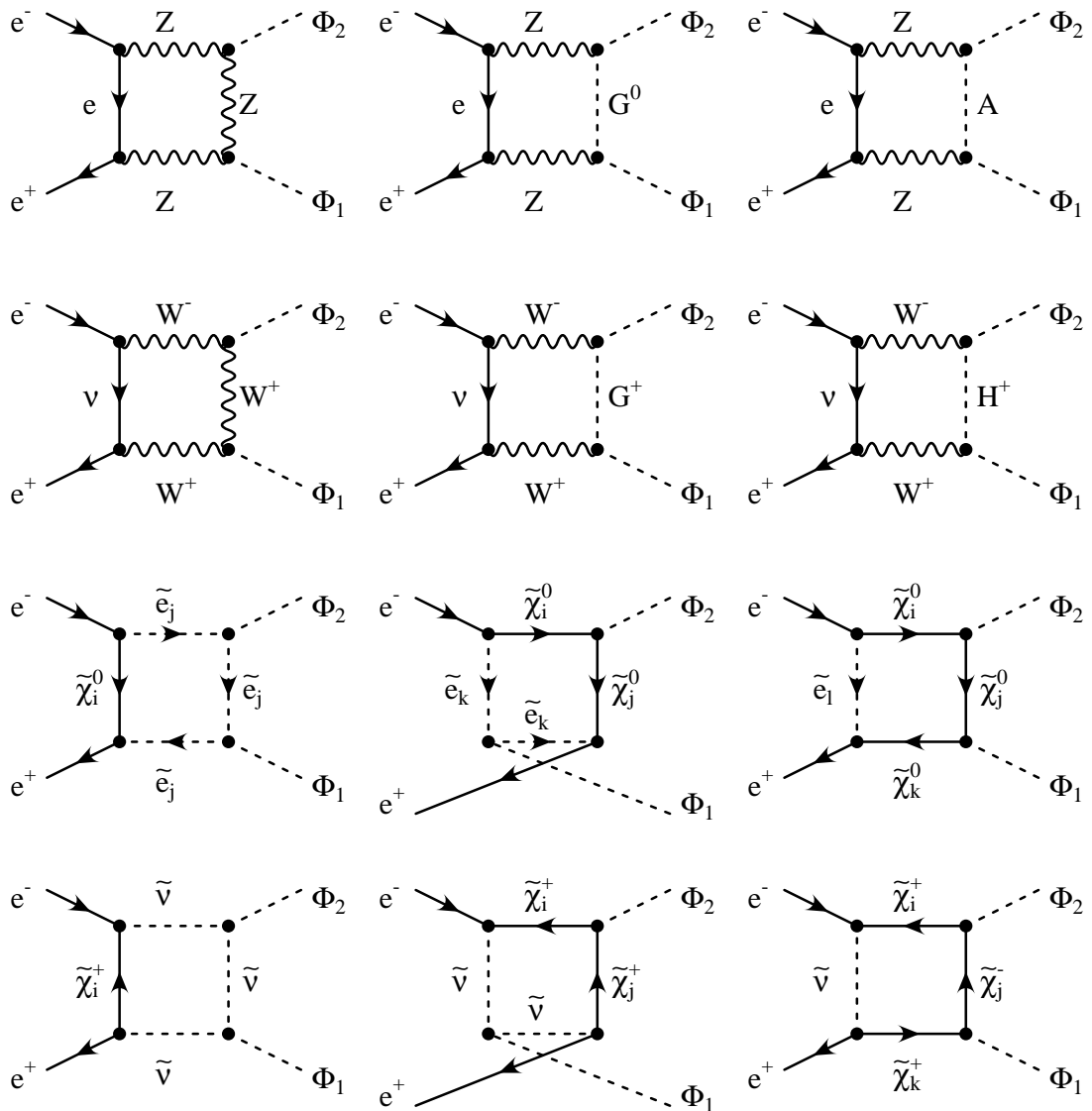


Fig. 1b

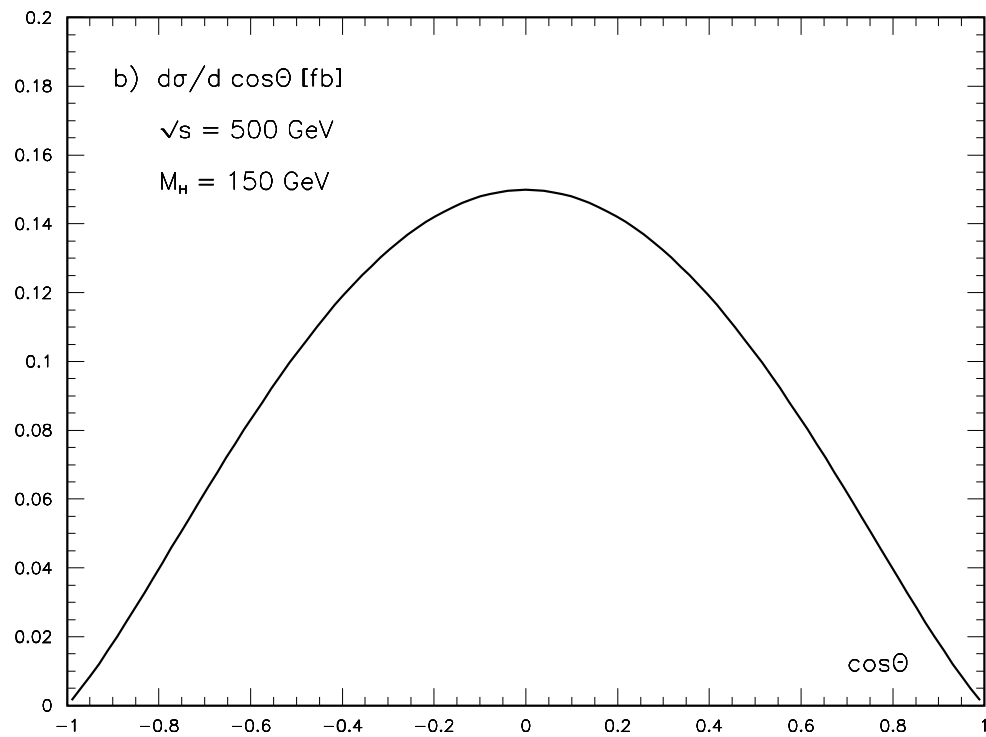
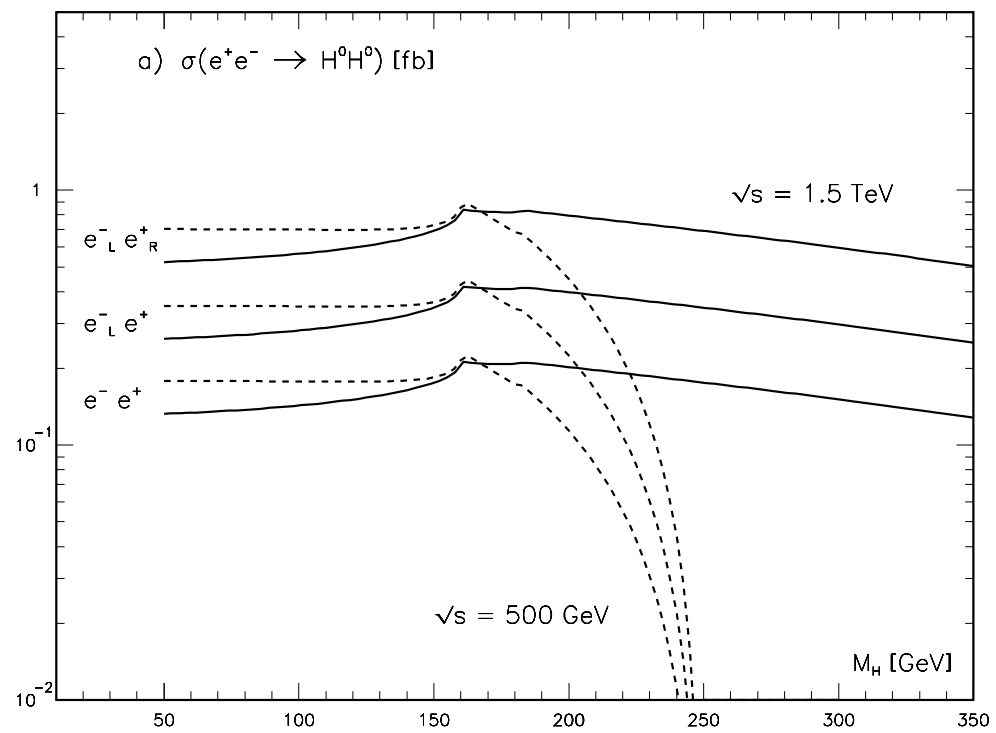


Fig. 2

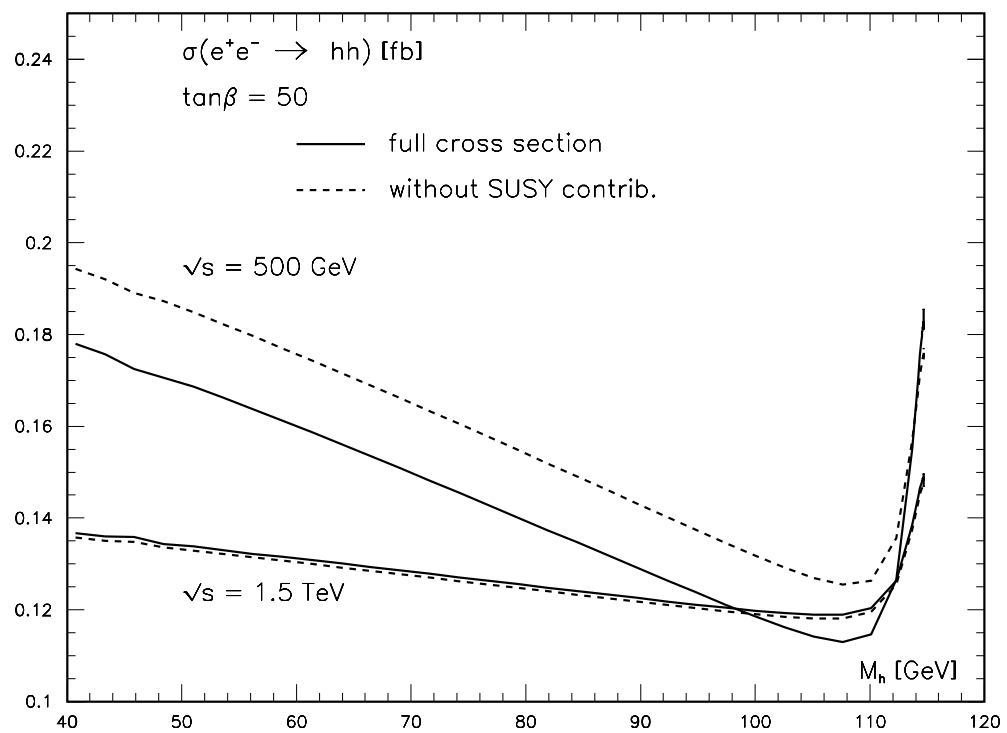
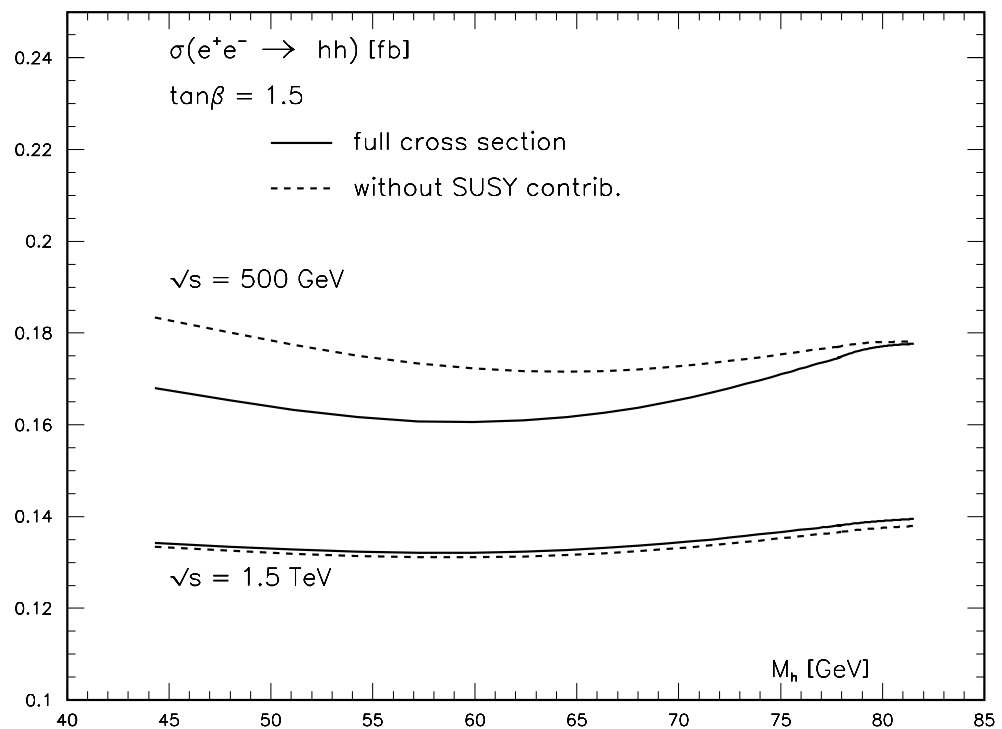


Fig. 3

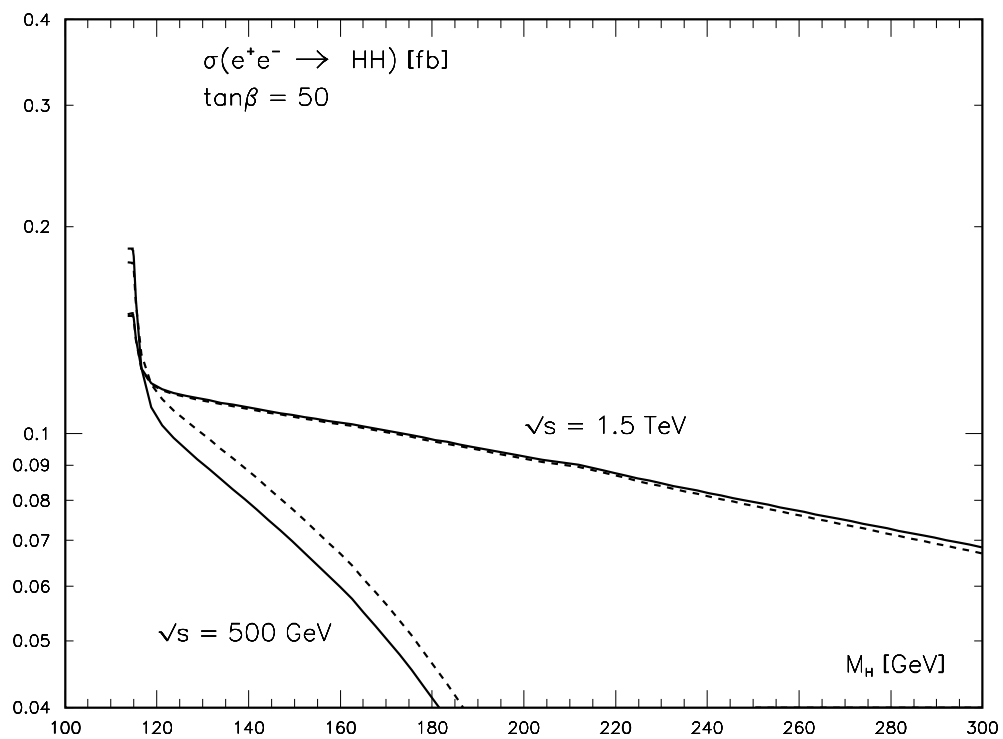
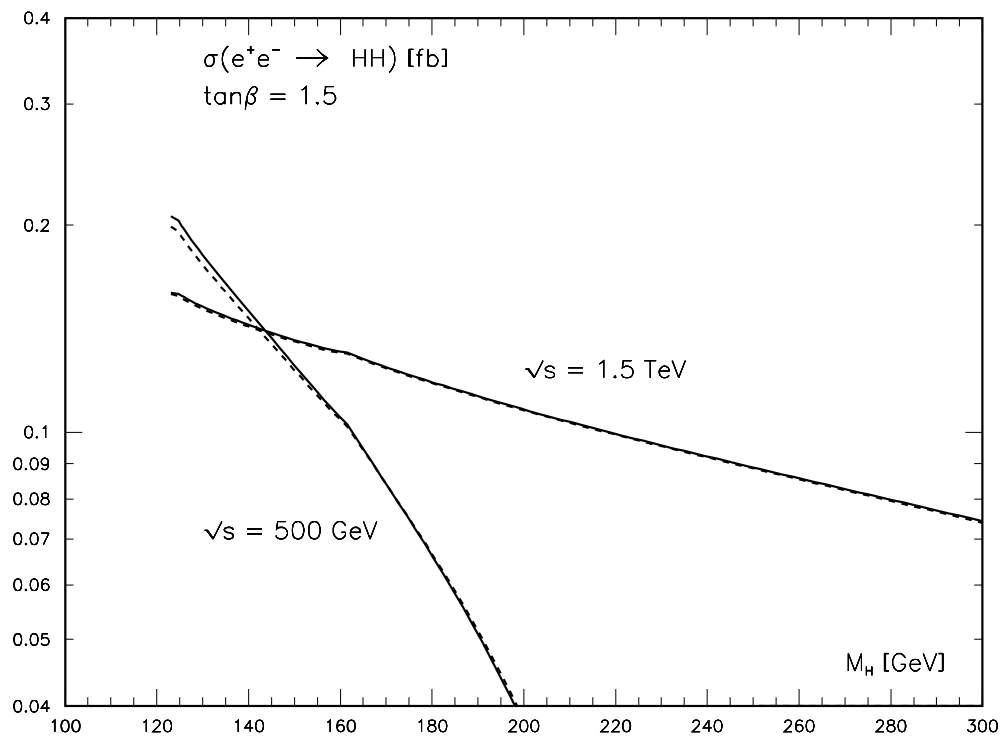


Fig. 4

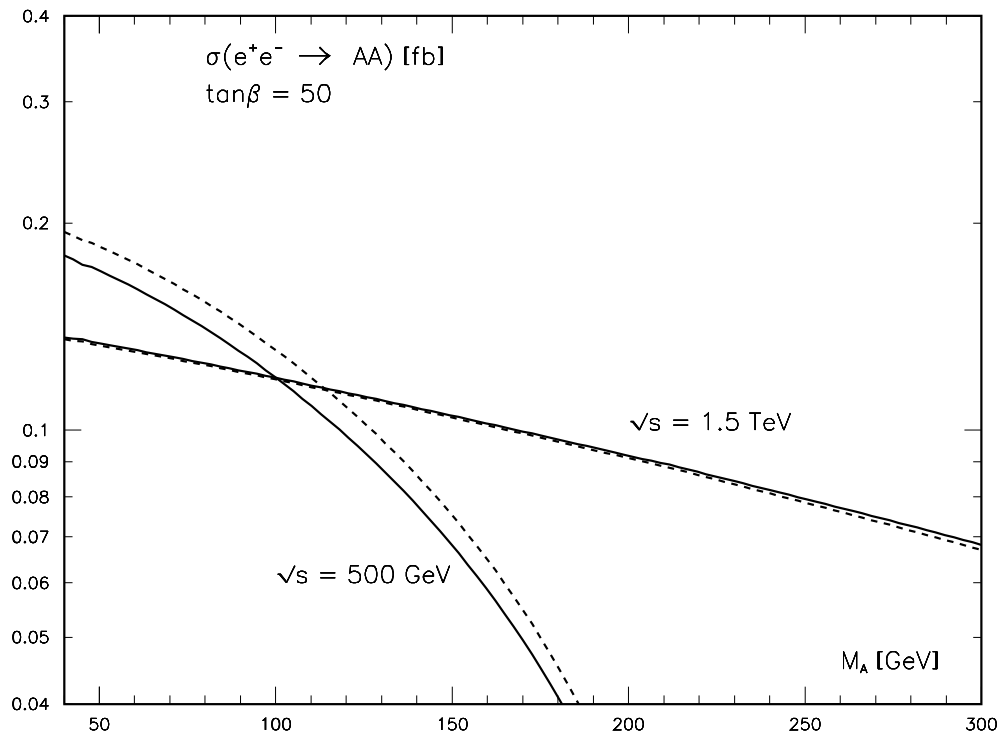
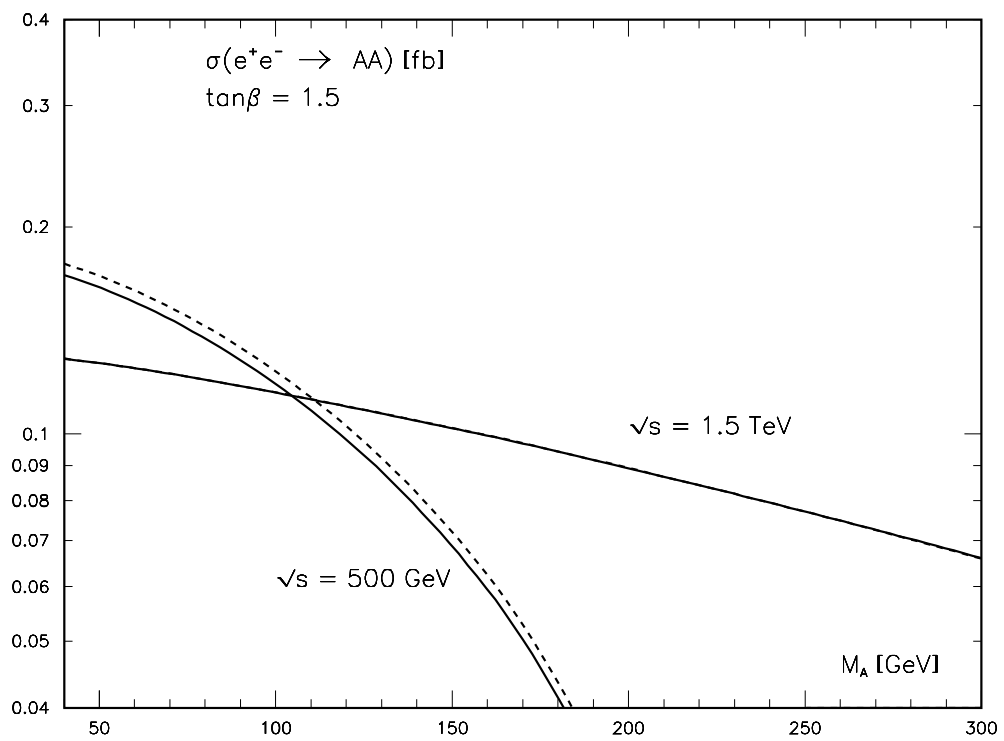


Fig. 5

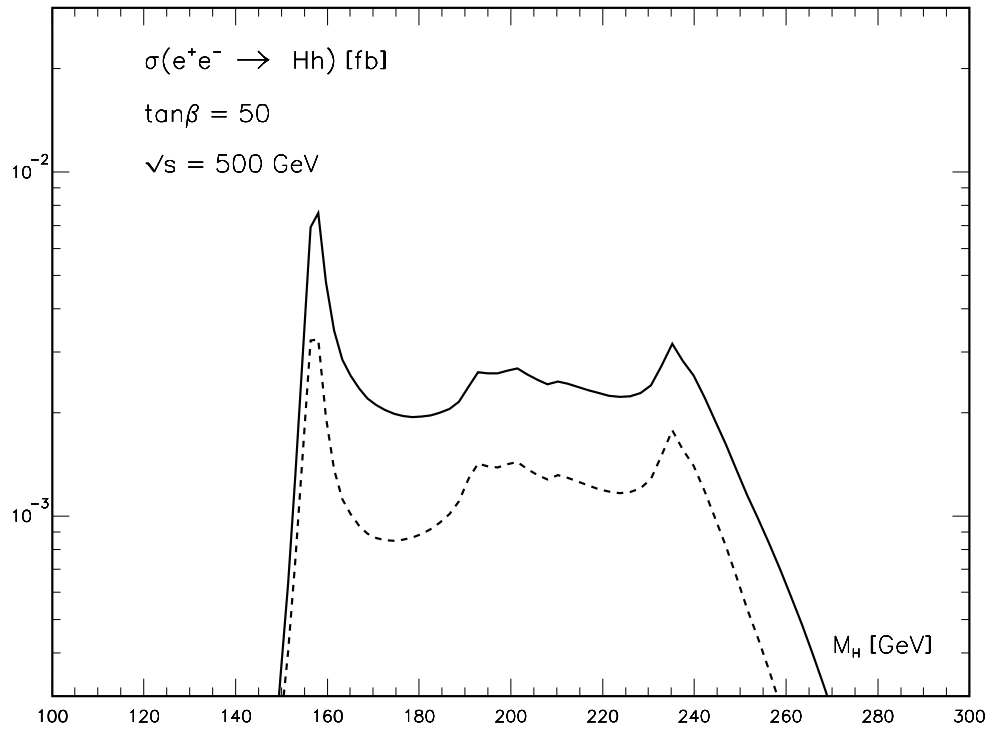
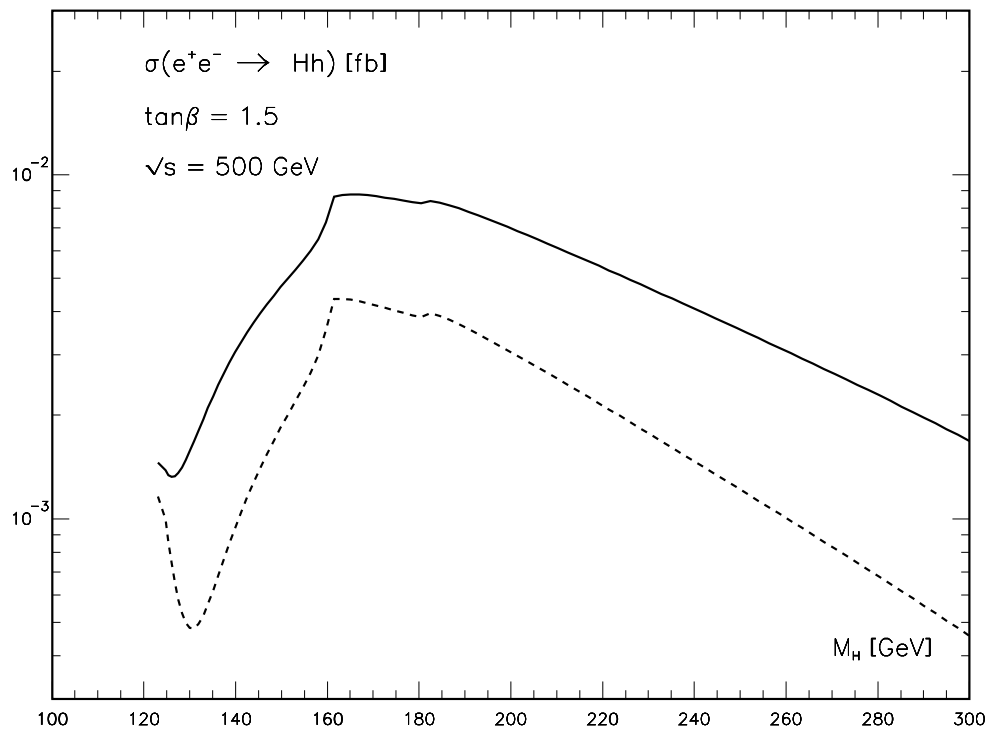


Fig. 6